

Microscopic dynamics of the evacuation phenomena

F.E. Cornes^a, G.A. Frank^c, C.O. Dorso^{a,b}

^a*Departamento de Física, Facultad de Ciencias Exactas y Naturales, Universidad de Buenos Aires, Pabellón I, Ciudad Universitaria, 1428 Buenos Aires, Argentina.*

^b*Instituto de Física de Buenos Aires, Pabellón I, Ciudad Universitaria, 1428 Buenos Aires, Argentina.*

^c*Unidad de Investigación y Desarrollo de las Ingenierías, Universidad Tecnológica Nacional, Facultad Regional Buenos Aires, Av. Medrano 951, 1179 Buenos Aires, Argentina.*

Abstract

We studied the room evacuation problem within the context of the Social Force Model. We focused on a system of 225 pedestrians escaping from a room in different anxiety levels, and analyzed the clogging delays as the relevant magnitude responsible for the evacuation performance. We linked the delays with the clusterization phenomenon along the *faster is slower* and the *faster is faster* regimes. We will show that the *faster is faster* regime is characterized by the presence of a giant cluster structure (composed by more than 15 pedestrians), although no long lasting delays appear within this regime. For this system, we found that the relevant structures in the *faster is slower* regime are those blocking clusters that are somehow attached to the two walls defining the exit. At very low desired velocities, very small structures become relevant (composed by less than 5 pedestrians), but at intermediate velocities ($v_d \simeq 3$ m/s) the pedestrians involved in the blockings increases (not exceeding 15 pedestrians).

Keywords:

Emergency evacuation, Social force model, Blocking clusters, Clogging delays

PACS: 45.70.Vn, 89.65.Lm

1. Introduction

The problem of emergency evacuations has become relevant in the last decades due to the increasing number and size of mass events (religious

events, music festivals, etc). The evacuation through narrow pathways or doorways appears as one of the most problematic scenarios in the literature. Many experiments and numerical simulations have been carried out for a better understanding of the crowd behavior in a variety of situations. The door width [1–9], the crowd composition [6, 10], or even the position of the exit [2, 11] raise as relevant magnitudes affecting the evacuation performance. The environmental and contextual realism, the pressure level, the occupancy density, the sample size, etc. are some inherent limitations of their experiments. Thus, the comparison between the results of the controlled experiments and the emergency escape behavior is quite controversial [1].

Ethical requirements in experimental setting impedes reproduce a real emergency situation. In this sense, the form that experimental researchers simulates a competitive scenario differs from one to another experiment. Therefore, many controlled experiments on the pedestrians’ egress time show dissimilar results. For instance, Refs. [4, 12, 13] report that under a simulated competitive scenario (say, allowing the contact between the pedestrians), the more the pedestrian’s anxiety to reach the exit, the greater the evacuation time. But other experimental reports provide evidence of decreasing evacuation times for increasing escaping desires [1, 6]. The former correspond to a “faster-is-slower” behavior, while the latter correspond to a “faster-is-faster” behavior. Whether the dominant behavior is “faster-is-slower” or “faster-is-faster” seems to be a matter of the pushing aggressiveness, in spite of the desire to reach the exit [1]. Thus, it has been proposed recently that the term “faster-is-slower” should be replaced by the more precise one: “aggressive egress-is-slower”.

The Social Force Model (SFM) introduced by Helbing [14] was the first model to accomplish a “faster-is-slower” effect for moderate to high anxiety levels within the crowd. This occurs whenever friction dominates the pedestrian dynamic [15–17]. The “faster-is-faster” phenomenon was also reported within this model, but for very high pressures among the individuals [17].

The time-lapse between consecutive evacuees and the egress curve are one of the most common measures for experimental and computational research [6–8, 11–13, 16, 17]. The egress curve shows that the leaving flow may occur either regularly or intermittently, depending on the pedestrians’ anxiety to reach the exit. Clogging can be observed as “arching structures” just

before any narrowing of the leaving pathway [14, 16–18]. Clogging has also been related to the pressure inside the *bulk* on this system [14, 16, 17, 19–24].

Our aim is to analyze the relation between the delays of consecutive leaving pedestrians and the topological structures among the crowd during the *faster is slower* and *faster is faster* regimes. The work is organized as follows. In Section 2 we introduce the dynamics equations for evacuating pedestrians, in the context of the Social Force Model (SFM). We also define the meaning of spatial clusters. Section 3 details the simulation procedures used to studying the room evacuation of a crowd under increasing anxiety levels. Section 4 displays the result of our investigation, while the conclusions are summarized in Section 5.

2. Theoretical background

2.1. The Social Force Model (SFM)

Our research was carried out in the context of the “social force model” (SFM) proposed by Helbing and co-workers [14]. This model states that human motion is caused by the desire of people to reach a certain destination at a certain velocity, as well as other environmental factors. It is a generalized force model, including socio-psychological forces, as well as “physical” forces like friction. These forces enter the Newton equation as follows.

$$m_i \frac{d\mathbf{v}^{(i)}}{dt} = \mathbf{f}_d^{(i)} + \sum_{j=1}^N \mathbf{f}_s^{(ij)} + \sum_{j=1}^N \mathbf{f}_g^{(ij)} \quad (1)$$

where the i, j subscripts correspond to any two pedestrians in the crowd. $\mathbf{v}^{(i)}(t)$ means the current velocity of the pedestrian (i), while \mathbf{f}_d and \mathbf{f}_s correspond to the “desired force” and the “social force”, respectively. \mathbf{f}_g is the granular force.

The “desired force” \mathbf{f}_d describes the pedestrians own desire to move at the desired velocity v_d . But, due to environmental factors (*i.e.* obstacles, visibility), he (she) actually moves at the current velocity $\mathbf{v}^{(i)}(t)$. Thus, he (she) will accelerate (or decelerate) to reach the desired velocity v_d that will make him (her) feel more comfortable. Thus, in the Social Force Model, the

desired force reads [14].

$$\mathbf{f}_d^{(i)}(t) = m_i \frac{v_d^{(i)} \mathbf{e}_d^{(i)}(t) - \mathbf{v}^{(i)}(t)}{\tau} \quad (2)$$

where m_i is the mass of the pedestrian i and τ represents the relaxation time needed to reach his (her) desired velocity. \mathbf{e}_d is the unit vector pointing to the target position. For simplicity, we assume that v_d remains constant during an evacuation process, but \mathbf{e}_d changes according to the current position of the pedestrian. Detailed values for m_i and τ can be found in Refs. [14, 25].

The ‘‘social force’’ $\mathbf{f}_s^{(ij)}$ represents the psychological tendency of any two pedestrians, say i and j , to stay away from each other (*private sphere* preservation). It is represented by a repulsive interaction force

$$\mathbf{f}_s^{(ij)} = A_i e^{(R_{ij}-r_{ij})/B_i} \mathbf{n}_{ij} \quad (3)$$

where (ij) represents any pedestrian-pedestrian pair, or pedestrian-wall pair. A_i and B_i are two fixed parameters (see Ref. [16]). The distance $R_{ij} = R_i + R_j$ is the sum of the pedestrians radius, while r_{ij} is the distance between the center of mass of the pedestrians i and j . \mathbf{n}_{ij} stands for the unit vector in the \vec{j} direction. For the case of repulsive feelings with the walls, d_{ij} corresponds to the shortest distance between the pedestrian and the wall [14, 26].

Any two pedestrians touch each other if their mutual distance r_{ij} is smaller than R_{ij} . Also, any pedestrian touches a wall if his (her) distance r_{ij} to the wall j is smaller than R_i . In these cases, an additional force is included in the model, called the granular force \mathbf{f}_g . It is composed by two forces: a sliding friction and a body force. The expression for this force is

$$\mathbf{f}_g^{(ij)} = \mathbf{f}_{sliding} + \mathbf{f}_{body} = \kappa_t g(R_{ij} - r_{ij}) (\Delta \mathbf{v}^{(ij)} \cdot \hat{\mathbf{t}}_{ij}) \hat{\mathbf{t}}_{ij} + \kappa_n g(R_{ij} - r_{ij}) \hat{\mathbf{n}}_{ij} \quad (4)$$

where κ_t and κ_n are fixed parameters. The function $g(R_{ij} - r_{ij})$ is equal to its argument if $R_{ij} > r_{ij}$ (*i.e.* if pedestrians are in contact) and zero for any other case. $\Delta \mathbf{v}^{(ij)} \cdot \hat{\mathbf{t}}_{ij}$ represents the relative tangential velocities of the sliding bodies (or between the individual and the walls).

Notice that the sliding friction occurs in the tangential direction while the body force occurs in the normal direction. Both are assumed to be linear with respect to the net distance between contacting pedestrians. The coefficients k_t (for the sliding friction) and k_n (for the body force) are supposed to be related to the areas of contact and the clothes material, among others.

2.2. Some definitions

In this section we define magnitudes which we have found useful in order to explore the system properties. We will focus our attention in two quantities

- In Section 2.2.1 we will define and characterize the concept of clustering structures.
- In Section 2.2.2 we will introduce the meaning of a clogging delay and we will explain different kinds of it.
- In Section 2.2.3 we will relate the clustering structures with clogging delays.

2.2.1. Clustering structures

Human clustering arises when pedestrians get in contact between each other. These morphological structures are responsible for the time delays during the evacuation process [15–17]. Thus, for future analysis a precise definition of this kind of structures is needed.

Clusters

Many previous works showed that clusters of pedestrians play a fundamental role during the evacuation process [15–17]. In this sense, researchers demonstrated that there exist a relation between them and the clogging up of people. Clusters of pedestrians can be defined as the set of individuals that for any member of the group (say, i) there exists at least another member belonging to the same group (j) in contact with the former. Thus, we define a *spatial cluster* (C_g) following the mathematical formula given in Ref. [27].

$$C_g : p_i \in C_g \Leftrightarrow \exists p_j \in C_g / r_{ij} < (R_i + R_j) \quad (5)$$

where (p_i) indicate the i th pedestrian and R_i is his (her) radius (shoulder width). This means that C_g is a set of pedestrians that interact not only

with the social force, but also with physical forces (*i.e.* friction force and body force).

Fig. 1a shows four spatial clusters. We will label a spatial cluster composed by n pedestrians as a n -*spatial cluster*. Isolated pedestrians (*i.e.* without contact with their surrounding individuals) corresponds to a 1-*spatial cluster* (green circles in Fig. 1a).

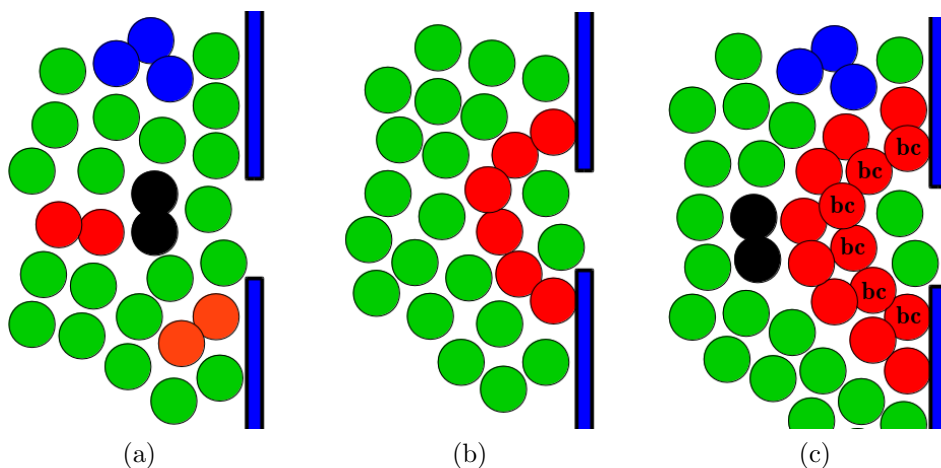


Figure 1: (a,b,c) Schematic representation of different spatial structures clusters. Each color represent a different spatial cluster. Isolated pedestrians are represented by green circles (1-spatial cluster). (a) Three 2-spatial cluster are represented by black, orange and red circles. One 3-spatial cluster is represented by blue circles. (b) One 6-spatial cluster is represented by red circles. This one corresponds to a blocking cluster. (c) Multiple spatial clusters founded through the simulations. 3-spatial cluster, 2-spatial cluster and 14-spatial cluster are represented by blue, black and red circles, respectively. Also, the 14-spatial cluster includes a blocking cluster (labeled as bc). The blue boxes represent the walls.

Blocking clusters

The simulations show that some spatial clusters are able to *block* the door. We will call *blocking cluster* to these kind of spatial clusters. In this sense, a “blocking cluster” is defined as the minimum subset of clustered particles (*i.e.* spatial cluster) closest to the door whose first and last component particles are in contact with the walls at both sides of the door [16].

Fig. 1b shows a typical blocking cluster composed by 6 pedestrians (red circles). As a special type of a spatial cluster, these can be composed by different number of pedestrians. Our simulations show that they can include from 5 to a maximum of 15 pedestrians for a door width of 0.92 m. Ref. [15] shows that this depends on door width.

A blocking cluster may coexist simultaneously with other spatial clusters. In this sense, we can observe in Fig. 1c three spatial clusters: 2, 3 and 14-spatial cluster are present in it. Notice that the blocking cluster belongs to a greater spatial cluster of 14 pedestrians. As we will see in Section 4.3, this occurs more frequently for high desired velocities.

2.2.2. Clogging delays

Clogging delays are a quite relevant quantity during the evacuation process. They are defined as the period of time between the egress of two consecutive pedestrians [15, 16, 25]. Animations shows that there are two generating mechanisms for a delay.

Frictional clogging delays

As stated in the last Section, blocking clusters are those spatial structures that block the exit. Refs. [15–17] show that they are responsible of worsening the evacuation performance. Thus, blocking clusters are one of the mechanism of production of a delay. In Fig. 2 we illustrate how this mechanism operates. Notice that the clogging delay starts when individual “1” left the room. At the same time (*i.e.*, $t = 0$ s), we can observe that individual “2” belongs to a blocking cluster, delaying his (her) outgoing. Later, at $t = 0.5$ s, it breaks and finally, individual “2” leaves the room at 1 s.

We conclude that the clogging delay of 1 s between individuals 1 and 2 was originated through a blocking cluster. In other words, the delay is a consequence of the granular forces between pedestrians. So, we define a *frictional clogging delay* as the clogging delays produce by a blocking cluster.

We remark that the frictional clogging delay consists of two contributions. One corresponds to the time that spends the individual jammed in the blocking cluster. And the other corresponds to the time lapse between

the breakup of the blocking structure and the exit time of the pedestrians (belonging to this blocking structure). This time corresponds to the *transit time* (0.5 s in Fig. 2).

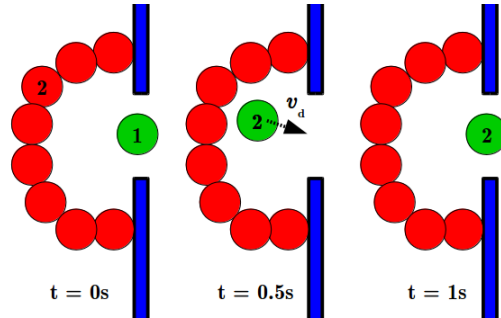


Figure 2: Schematic representation of the generating mechanism of a frictional clogging delay. The black line corresponds to the direction of the desired velocity v_d . A blocking cluster (red circles) impedes ind. 2 from leaving the room. It breaks at $t = 0.5$ s and finally, at $t = 1$ s he (she) escapes from the room. See text for more details.

Social clogging delays

Animations show that there exists another generating mechanism for a delay. On one side, this can occur without the presence of a blocking cluster, as we illustrate in Fig. 3a. As in Fig. 2, the delay of 1 s corresponds to the outgoing process between individuals 1 and 2. But, in this case, he (she) is delayed due to the presence of individual 1. Notice that this occurs due to the social force.

We stress the fact that this situations occur for low pedestrian density. This may be the case when the anxiety level is small and therefore, individuals do not each other. Thus, we can observe an unstable equilibrium between the desired force and the social force near the door.

On other side, we have the situation in which the social force delayed the outgoing of people can be reached through the breaking of a blocking cluster. We illustrate this mechanism in Fig. 3b. Again, a blocking cluster impedes many pedestrians to leave the room, particularly individuals labeled as 2 and 3. But, unlike Fig. 2, it releases two pedestrians after it breaks, like a *burst*, at $t = 0.5$ s. Notice that $t = 1$ s corresponds to the same situation showed in

Fig. 3a at $t = 0$ s. But, in this case the clogging delay of 0.3 s between 2 and 3 is shorter than the former (*i.e.*, $\Delta t = 1$ s). Finally, notice that the clogging delay of 1 s between individuals 1 and 2 corresponds to a frictional clogging delay (*i.e.*, produced by a blocking cluster).

Summarizing, we conclude that the clogging delay of 1 s and 0.3 s in Fig. 3a and Fig. 3b, respectively, was produced by the repulsion between pedestrians. In other words, the delay is a consequence of the social force between them. So, we define a *social clogging delay* as those clogging delays produced by the social interaction.

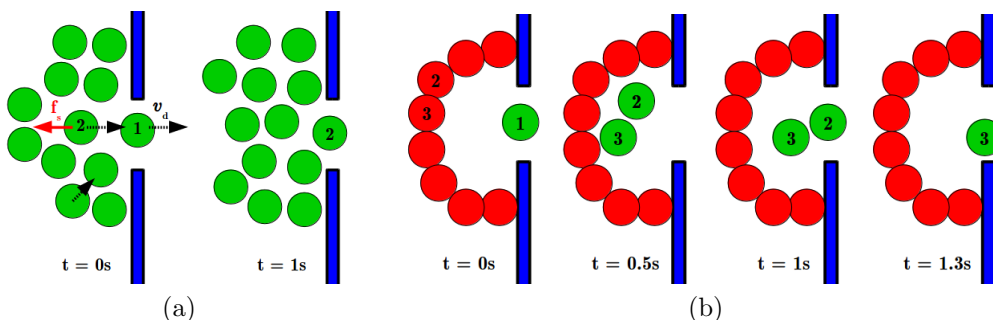


Figure 3: (a,b) Schematic representation of the production mechanism of a social clogging delay. Black lines correspond to the direction of the desired velocity v_d . The red continue line corresponds to the social force f_s exerted by individual “1” over “2”. Green (red) circles indicates that this pedestrian is (is not) in contact with his (her) surrounding individuals. (a) At $t = 0$ s, pedestrians cannot leave the room due to the presence of individual 1. When he (she) escapes, pedestrian labeled as 2 leaves the room at 1 s. (b) A blocking cluster (red circles) impedes individual 2 and 3 (among others) to leave the room. It breaks at $t = 0.5$ s and later, at $t = 1$ s, individual 2 escapes from the room. Finally, pedestrian 3 escapes at $t = 1.3$ s. The social clogging delay corresponds to the time lapse between individual 2 and 3 (*i.e.* $\Delta t = 0.3$ s). Again, delay of 1 s between pedestrians 1 and 2 corresponds to a frictional clogging delay.

2.2.3. Arch-clogging correlation coefficient

In order to quantify the relationship between blocking cluster and clogging delay we define the arch-clogging correlation coefficient as follows [16]

$$c_{ac} = \frac{1}{N} \sum_{cd=1}^N f(t_2^{bc}, t_1^{cd}, t_2^{cd}), \quad (6)$$

Table 1: Computation of the arch-clogging correlation coefficient c_{ac} (Eq. 6) in the case of Figs. 2 and 3.

Fig.	Pairwise (i,j)	t_1^{cd} (s)	t_2^{bc} (s)	t_2^{cd} (s)	$f^{(i,j)}$	Δt (s)	clogging type
2	(1,2)	0	0.5	1	1	1	frictional
3a	(1,2)	0	-	1	0	1	social
3b	(1,2)	0	0.5	1	1	1	frictional
3b	(2,3)	1	-	1.3	0	0.3	social

where N is the total number of clogging delays during the reported time interval, t_2^{bc} corresponds to the time stamp for the blocking cluster breaking and t_1^{cd} (t_2^{cd}) corresponds to the time stamp for the delay beginning (ending). The function f is equal to 1 if $t_1^{cd} \leq t_2^{bc} \leq t_2^{cd}$, and zero otherwise. This means that f is equal to 1 if the outgoing individual belonged to a blocking cluster during the interval (t_1^{cd}, t_2^{cd}) . Table 1 resumes the diagrams shown in Figs. 2 and 3.

This correlation c_{ac} represents the fraction of *frictional clogging delays* (or *social clogging delays*) with respect to all the clogging delays appearing during the (stationary) evacuation process. Any value close to one indicates that most of the clogging delays belong to blocking clusters. On the contrary, if c_{ac} is close to zero, most of them belong to social force interactions.

3. Numerical simulations

The simulations were performed on a 20 m \times 20 m square room with 225 pedestrians inside. The occupancy density was set to 0.6 people/m², as suggested by healthy indoor environmental regulations [28]. The room had a single exit on one side, placed in the middle of it in order to avoid corner effects. The door width was $L = 0.96$ m, enough to allow up to two pedestrians to escape simultaneously (side by side).

The pedestrians were modeled as soft spheres. They were initially placed in a regular square arrangement along the room with random velocities, resembling a Gaussian distribution with null mean value. The rms value for the Gaussian distribution was close to 1 m/s. The desired velocity v_d was

the same for all the individuals. At each time-step, however, the desired direction \mathbf{e}_d was updated, in order to point to the exit.

We used periodic boundary condition (re-entering mechanism) for the outgoing pedestrians. That is, those individuals who were able to leave the room were reinserted at the back end of the room and placed at the very back of the bulk with velocity $v = 0.1$ m/s, in order to cause a minimal bulk perturbation. This mechanism was carried out in order to keep the crowd size unchanged, and therefore, the pressure among pedestrians.

According to the literature (see Ref [14]), the model parameters used were $\tau = 0.5$ s, $A = 2000$ N, $B = 0.08$ m and $\kappa_t = 2.4 \times 10^5$ kg m⁻¹ s⁻¹. However, the pedestrian’s mass and radius were set according to the more realist values of 70 kg and 0.23 m, as in Ref. [29]. Also, the compression coefficient κ_n was set equal to 2.62×10^4 N m⁻¹, according to the experimental value of the human torso stiffness [30].

The simulations were performed using LAMMPS molecular dynamics simulator with parallel computing capabilities [31]. The time integration algorithm followed the velocity Verlet scheme with a time step of 10^{-4} s. We implemented special modules in C++ for upgrading the LAMMPS capabilities to attain the “social force model” simulations. We also checked over the LAMMPS output with previous computations (see Refs. [15, 16]).

Data recording was done at time intervals of 0.05τ , that is, at intervals as short as 10% of the pedestrian’s relaxation time. The simulating process lasted until 7000 pedestrians left the room.

The explored anxiety levels ranged from relaxed situations ($v_d = 1$ m/s) to highly stressing ones ($v_d = 10$ m/s). This last value can hardly be reached in real life situations. However, in Ref. [17], it was shown that similar pressure levels can be reached in a big crowd with a moderate anxiety level. Thus, this wide range of desired velocities allows us to study different pressure scenarios. We also assumed that the pedestrians were not able to fall due to the crowd pressure as in Ref. [30].

4. Results

Our results run along four major streams as follows:

- In Section 4.1 we revisit the context of the evacuation time. We further introduce other novel concepts that will be used throughout the work.
- In Section 4.2 we show the differences between the *faster is slower* and *faster is faster* regimes in terms of the clogging delays.
- In Section 4.3 we focus on the clusterization phenomenon at either the *faster is slower* and *faster is faster* regimes.
- In Section 4.4 we analyze the relationship between the size of the clustering structures and the corresponding clogging delays.

4.1. A review of the evacuation processes at bottlenecks

The evacuation time versus the desired velocity

As a first step, we computed the evacuation time for a wide range of desired velocities v_d . This is shown in Fig. 4. We stress the fact that the explored range corresponds to the one analyzed by Sticco *et. al.* (see Ref. [17]) but, considering periodic boundary conditions. This means that any pedestrian who left the room is introduced on the opposite side of the bottleneck (see Section 3).

It can be seen in Fig. 4 the *faster is slower* (blue circles) and the *faster is faster* (white and yellow circles) phenomena as reported in Ref. [17]. Recall that the *faster is slower* regime, introduced by Helbing *et. al.* [14] corresponds to the increase in the evacuation time as the pedestrian's anxiety level increases. Thus, the evacuation efficiency reduces within this region. It was shown in Ref. [15] that this is related to the presence of sliding friction among pedestrians (and the walls).

Besides, it was reported in Ref. [17] that the evacuation time decreases for very high desired velocities (*i.e.*, high pressures). This behavior corresponds to the *faster is faster* regime. It was concluded (see Ref. [17]) that as the crowd pushing force increases, the sliding friction at the “blocking cluster”

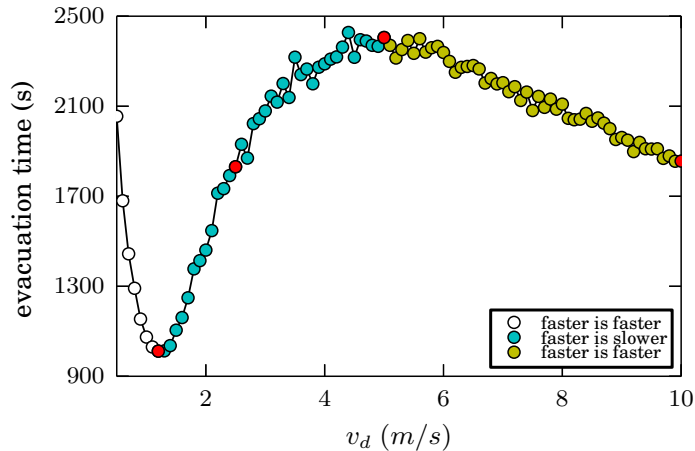


Figure 4: Evacuation time for the first 7000 evacuees as a function of the desired velocity v_d . The simulated room was $20\text{ m} \times 20\text{ m}$ with a single door of 0.92 m (say, the diameter of two pedestrians). The number of individuals inside the room was 225. This curve was computed from a single simulation process. Re-entering mechanism was allowed (see text for more details). The simulation lasted until 7000 individuals left the room. Desired velocities of $v_d = 1.2, 2.5, 5.0$ and 10.0 m/s are indicated in red color.

seems not enough to prevent this kind of structure from (completely) stopping the crowd movement. This is the reason for the improvement of the evacuation time at the exit. We call the attention that we are not considering the possibility of fallen pedestrians due to high pressures (see Ref. [30] for details). Further readings on the role of the sliding friction can be found in Refs. [15–17].

As can be noticed from Fig. 4, the *faster is slower* regime appears for desired velocities between 1 and 5 m/s (approximately). This is somewhat shifted from the range reported in Ref. [17] ($2 < v_d < 8\text{ (m/s)}$, approximately). The same occurs for both *faster is faster* effects. This discrepancy is a consequence of the periodic boundary condition. The *bulk* pressure remains (almost) constant during the stationary state for periodic boundary condition. But, it decreases for non-periodic conditions, since pedestrians escape from the room. This phenomenon is similar the one observed in Ref. [17] when varying the number of pedestrians inside the room.

We will focus on four specific desired velocities in the next section. These

correspond to the minimum evacuation time ($v_d = 1.2$ m/s), the maximum evacuation time ($v_d = 5$ m/s) and two desired velocities with similar evacuation times but on different regimes. The desired velocities $v_d = 2.5$ m/s and $v_d = 10$ m/s were chosen as representative of the *faster is slower* and *faster is faster* phenomena, respectively.

Discharge curves

We proceed to a first microscopic analysis of the evacuation process through the discharge curves (say, the number of individuals that escape from the room over time). Fig. 5 shows the discharge curves for four desired velocities (see caption for details) [15–17]. For each curve, the time between consecutive evacuees (*i.e.* the delay) is represented by a horizontal line.

It can be seen in Fig. 5 that the evacuation time for the first 180 evacuees corresponds to the upper end of each discharge curve. It can be seen that the desired velocities $v_d = 1.2$ and 5 m/s correspond to the minimum and maximum evacuation time, respectively (say, 25 s and 65 s, approximately). The curves for $v_d = 2.5$ and 10 m/s meet at the top of the figure, as expected from Fig. 4. But most interesting, it can be noticed an increase in the duration of the delays (represented by horizontal segments) from the curve on the left to one on the right in Fig. 5. It is worth mentioning that the evacuation time corresponds to the sum of all delays, and thus, the increase in evacuation time is related to the increase in the duration of delays. The relationship between evacuation time and delays will be further analyzed in more detail in the next section.

A statistical test on the (global) uniformity of the discharge curves was done in Appendix A. It could be established that the flow of evacuees is not uniform at the *faster is slower* and *faster is faster* regimes (within a significance of 5%). However, a tendency towards uniformity could be noticed (at least) for the *faster is faster* regime as the individual’s anxiety level (v_d) increases.

In summary, the discharge curves show that the pedestrian flow is never uniform (within a significance level), but delays tends to become more regular for very high anxiety levels (or *bulk* pressures).

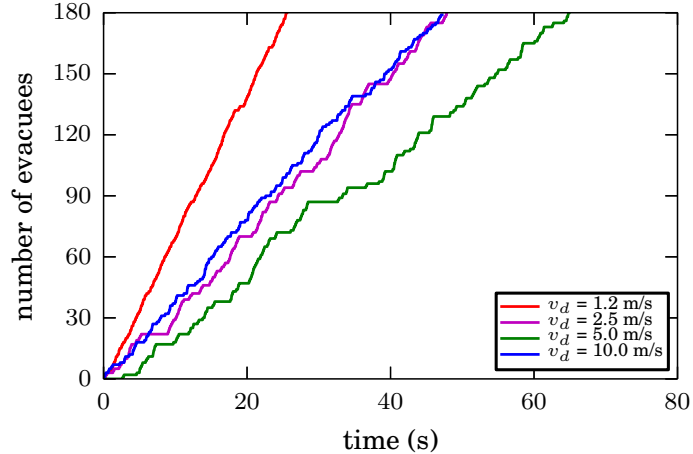


Figure 5: Number of pedestrians that left the room versus time, for four different desired velocities v_d (see legend). The showed time-window corresponds to a representative sample of 180 pedestrians that left the room from a set of 7000 evacuees. The analyzed desired velocities are indicated by red circles in Fig. 4. The curves were computed from a single simulation process (re-entering mechanism was allowed)

4.2. Clogging delays analysis

In this section we turn to study the mechanism by which different types of clogging delays are generated. We analyze the clogging delays distributions and the contribution of each type of delay to the overall evacuation time.

4.2.1. Production mechanism of a delay

As mentioned in Section 2.2.2, there are two categories of clogging delays. The first one corresponds to those generated as a consequence of the social force among individuals (see Fig. 3). The second one corresponds to those that occur due to blocking clusters (see Fig. 2). The former corresponds to a *social clogging delay*, while the latter corresponds for a *frictional clogging delay*. Fig. 6 plots the coefficient c_{ac} (see Eq. 6) as a function of the clogging delays longer than (or equal to) any threshold t_c .

According to Fig. 6, the probability of finding frictional delays increases among long delays. In other words, long lasting delays commonly belong to blocking clusters. Thus, we can (almost) exclusively classify any delay longer

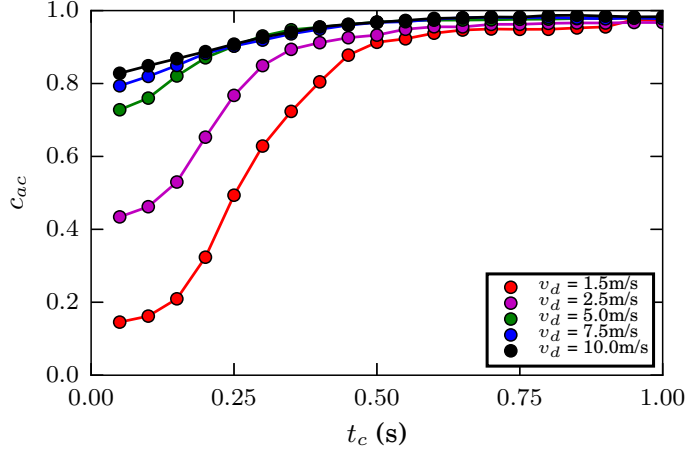


Figure 6: Arch-clogging correlation coefficient c_{ac} as a function of the duration of the delay (equal or greater than t_c) for five different desired velocities (see legend for details). All the curves were computed from a single simulation process (re-entering mechanism was allowed). We computed 6999 clogging delays for each desired velocity, according to the evacuation of 7000 pedestrians.

than 1 s as a *frictional clogging delay*. Notice that this criterion is fulfilled regardless of the value of the desired velocity v_d (within the explored range). The situation for short clogging delays appears somewhat mixed. Not all delays less than 1 s belong to a blocking cluster.

Furthermore, the fraction of frictional delays increases for increasing desired velocities (see Fig. 3). Recall from Appendix B that the probability of blocking clusters also increases for increasing values of v_d . This is the reason for the increase of the fraction of frictional clogging delays when increasing the desired velocity.

A careful examination of the evacuation animations shows that social delays may also appear after the breaking process of a blocking cluster. This corresponds to the *burst* released after the rupture, as exhibit in Fig. 3b. We observed in the animations (not shown) that this phenomenon occurs commonly as the desired velocity increases. Therefore, social delays should not be considered as “opposed” to frictional delays, but complementary to these.

The major conclusion from this Section is that long delays (say, greater than 1 s) can be associated to blocking clusters. But, those delays of short duration may either be associated to social interactions or granular interactions.

Our next step focuses on the relevance of the frictional and social clogging delays on the evacuation time. We computed the evacuation time considering these two categories of delays separately. Fig. 7 shows the results.

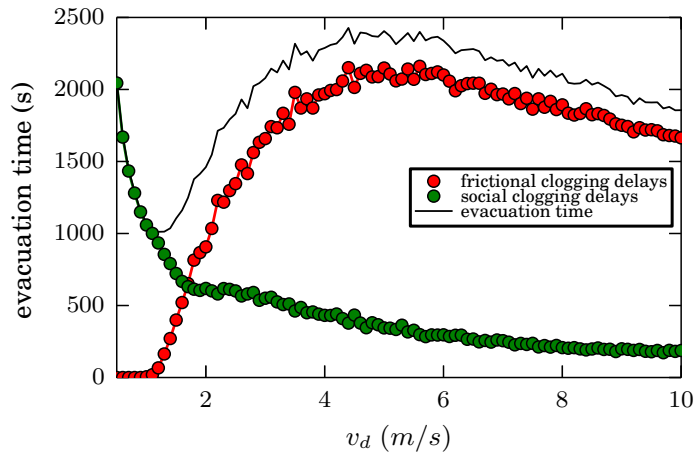


Figure 7: Evacuation time for the first 7000 evacuees as a function of the desired velocity v_d . The black line corresponds to the total evacuation time. Red and green circles correspond to the evacuation time associated with frictional and social clogging delays, respectively. These were recorded from a single simulation process (re-entering mechanism was allowed).

The evacuation time considering (adding) only the frictional delays (and thus the blocking clusters) is qualitatively similar to the total evacuation time. This corresponds to (almost) the entire explored interval ($v_d > 1.2$ m/s). However, this vanishes for $v_d < 1.2$ m/s. Recall that people are very seldom in contact between each other at such low desired velocities, and therefore, no blocking clusters are present (see Appendix B).

The evacuation time associated to the social delays (*i.e.* social clogging delays) decreases monotonically as the desired velocity increases. As men-

tioned above, the individuals are very seldom in contact for $v_d < 1.2$ m/s (see Fig. 3a). Notice that the total evacuation time and the social evacuation time coincide for $v_d < 1.2$ m/s, but no *faster is slower* effect takes place for the latter at higher v_s 's (as expected).

4.2.2. Clogging delay distributions

We further computed the delays's probability distribution, as shown in Fig. 8. We chose the same desired velocities as in Section 4.1 for the purpose of comparison. The distribution corresponding to all the clogging delays and the *frictional clogging delays* can be seen in red and blue bars, respectively. The latter corresponds to a subset of the former. Notice that distributions are valid for the specific door width mentioned in the caption (see Ref. [16] for more details).

The delays shorter than 3 s in Fig. 8 (approximately) are present in all the plotted situations. But, clogging delays greater than 3 s occur only for the intermediate situations $v_d = 2.5$ and 5 m/s (see Figs. 8b and 8c). Both situations exhibit delays up to 7 s approximately. Recall that these levels of v_d correspond to the *faster is slower* regime (see Fig. 4). The *faster is slower* regime includes long delays, while the *faster is faster* regime stands for delays no longer than 3 s (under the explored conditions).

4.2.3. Relevance of the clogging delays

We concluded in Section 4.2.1 that almost all the delays longer than 1 s correspond to the presence of a blocking cluster. Therefore, they correspond to *frictional clogging delays*. In Section 4.2.2 we further noticed that long delays (greater than 3 s) appear during the *faster is slower* regime. We focus on three categories: short ($\Delta t \leq 1$ s), intermediate ($1 \text{ s} < \Delta t \leq 3$ s) and long ($\Delta t > 3$ s) delays. Fig. 9 shows the evacuation time for these types of delays.

- Short clogging delays ($\Delta t \leq 1$ s): This kind of delays are the only relevant ones for desired velocities below 1.2 m/s. We already mentioned in Appendix B that no relevant blocking clusters appear at these desired velocities, and thus, all the clogging delays correspond to *social clogging delays*. Also, as can be seen this kind of delay does not allow

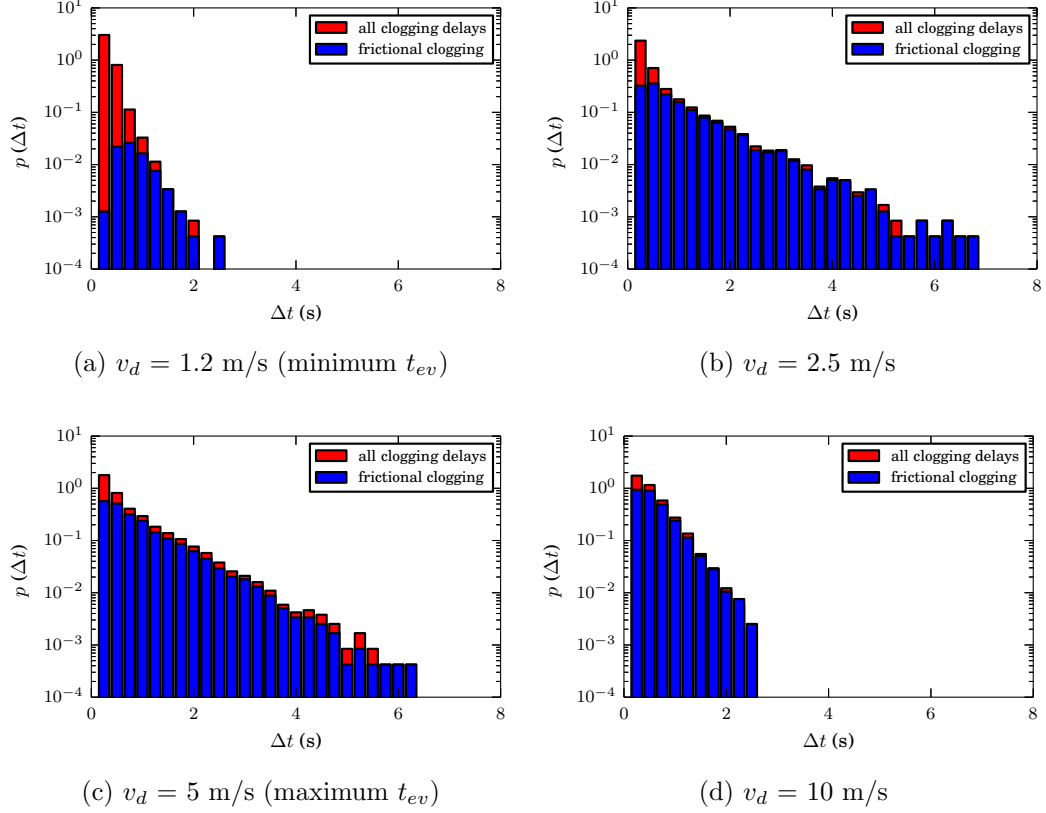


Figure 8: Normalized distributions of time lapses Δt between egresses of consecutive pedestrians up to 7000 people evacuated, for the same values of v_d analyzed in Fig. 5. The bin size is 0.25 s. Clogging delays and delays originated due to a blocking cluster (named frictional clogging) are indicated by red and blue bars, respectively. Frictional clogging corresponds to a subset of the clogging delays (see text for details). Thus, red bars are plotted behind the blue bars. The distribution area corresponding to the clogging delays is 1. Data was recorded after the first 10 s of the beginning of the simulation process, in order to avoid non-stationary effects. The door width was 0.92 m (say, the diameter of two pedestrians).

us to distinguish the *faster is slower* and *faster is faster* regimes (above 1.2 m/s).

- Intermediate clogging delays ($1 \text{ s} < \Delta t \leq 3 \text{ s}$): This category becomes relevant for $v_d > 1.2$ m/s. Their qualitative behavior for $v_d > 1.2$ m/s

is similar to the total evacuation time. Thus, unlike the short clogging delays, these are a good observable to identify the *faster is slower* and *faster is faster* regimes. Also, the cumulative time due to both delays explains almost all of the evacuation time.

- Long clogging delays ($\Delta t > 3$ s): They are only present for velocities between 1 and 7 m/s (as we mentioned in Section 4.2.2). As can be seen, these delays are not decisive for the presence of the *faster is slower* effect. Also, the lack of long clogging delays may be partially responsible for the *faster is faster* phenomenon.

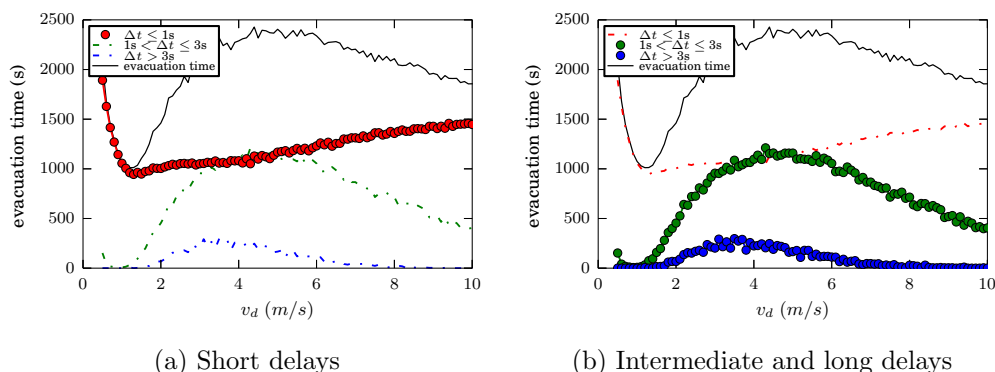


Figure 9: The black line corresponds to the evacuation time for the first 7000 evacuees as a function of the desired velocity v_d . Red, green and blue circles (and dashed lines) correspond to the different delay categories.

The following conclusions can be outlined from this Section. The analysis of the delays show that the overall evacuation time is mainly due to *frictional clogging delays* for $v_d > 2$ m/s. Also, the slope of the intermediate clogging delays ($1 \text{ s} < \Delta t \leq 3$ s) allows us to distinguish between the *faster is slower* and *faster is faster* regimes (see Fig. 9).

4.3. Clustering structure analysis

In this section we turn to study the clustering structures. We analyze the different kind of spatial clusters and we explore how they change with the desired velocity.

4.3.1. The morphology in the bulk of the crowd

Fig. 10 shows four snapshots of the *bulk* close to the exit. The shown situations correspond to the same desired velocities as in Section 4.2. Red and white circles represent the blocking and spatial clusters, respectively. We stress that the individuals in red (blocking cluster) also belong to the spatial cluster (white color) (see Fig. 10).

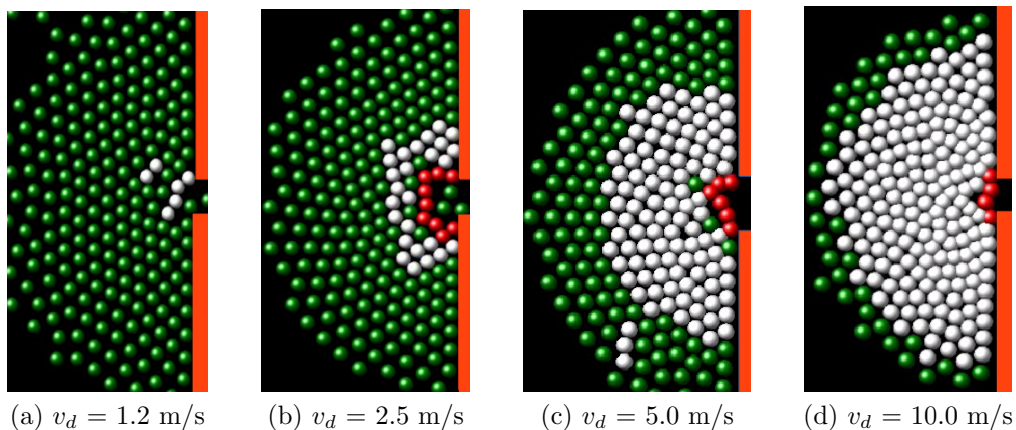


Figure 10: Snapshots of the *bulk* for four desired velocities. Red and white circles represent the blocking cluster and the spatial clusters, respectively. Green circles correspond to individuals without contact with his (her) surrounding pedestrians and walls. The orange lines represent the walls on the right of the room. The simulated room was $20\text{ m} \times 20\text{ m}$ with a single door of 0.92 m (say, the diameter of two individuals). The number of individuals inside the room was 225. The selected desired velocities are those indicated in red in Fig. 4.

As can be seen in Fig. 10, the number of individuals in contact increases with increasing desired velocities. This is the expected picture for people pushing towards the exit. The harder they push (increasing values of v_d), the larger the clogging region.

Notice that two small spatial clusters appear at $v_d = 1.2\text{ m/s}$ (see white circles in Fig. 10a). But these merge into a single spatial cluster of size 35, as the desired velocity increases to $v_d = 2.5\text{ m/s}$. However, it can be noticed that 4 individuals (green circles in Fig. 10b) remain out of contact with their closest neighbors. This is a rather common phenomenon for low desired velocities, as we were able to observe in the animations (not shown).

Interesting, Fig. 10b, also shows a burst of 3 individuals escaping from the room. These correspond to the breaking of a (former) blocking cluster (not shown). Therefore, this is associated to a social clogging delay. Also, the snapshots in Figs. 10c and 10d show a significant change in the size relation between the blocking cluster and the spatial cluster for increasing desired velocities. The ratio between this magnitudes is shown in Fig. 11.

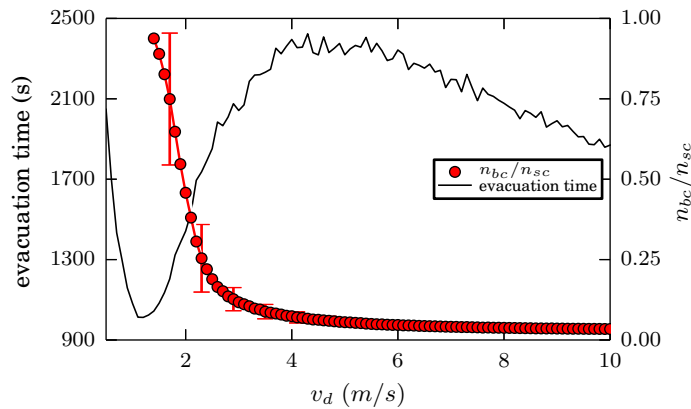


Figure 11: The black line corresponds to the evacuation time for 7000 evacuees, while the red circles correspond to the normalized size of a blocking cluster (n_{bc}) with respect to the spatial cluster (n_{sc}), both as a function of the desired velocity v_d . The spatial cluster corresponds to those in contact with the blocking cluster. The size of the blocking cluster and the spatial cluster were recorded every 0.05 s. The acquisition was done only when a blocking cluster existed. The error bars corresponds to $\pm\sigma$ (one standard deviation). These were computed from a single simulation process (re-entering mechanism was allowed).

A sharp decay in the blocking-to-spatial ratio can be noticed in Fig. 11. We immediately identify two regimes according to Fig. 11. For $v_d < 3$ m/s (approximately), the size of the blocking cluster is seemingly of the same order as that of the spatial cluster. For $v_d > 3$ m/s, instead, the size of the blocking cluster becomes negligible with respect to that of the spatial cluster.

We will next turn to study in more detail the size of the spatial cluster.

4.3.2. Size of spatial clusters

Recall that as the desired velocity increases, more people gets into contact with each other, and therefore, the size of the spatial cluster increases for increasing anxiety levels of the individuals. We classified the spatial clusters into three categories (according to their size n) as follows: small ($1 < n \leq 5$), medium ($5 < n < 15$) and big ($n \geq 15$). We remark that the medium category corresponds to the commonly observed size of the blocking clusters. Fig. 12 shows the (normalized) number of spatial clusters for each category (see caption for details). We will analyze each category separately.

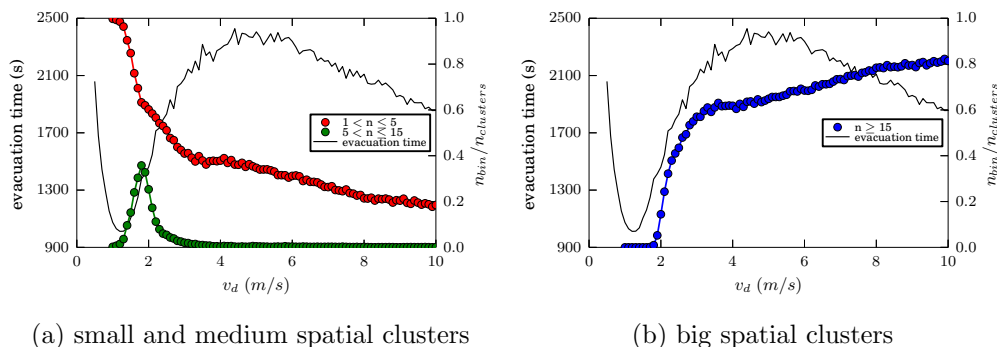


Figure 12: (a,b) The black line corresponds to the evacuation time for the first 7000 evacuees, while the red, green and blue circles correspond to the normalized number of spatial clusters (n_{bin}) for three different size categories (see legend for details), as a function of the desired velocity v_d . The normalization was done with respect to the total number of spatial clusters ($n_{clusters}$). The size of each spatial cluster was obtained every 0.05 s. Data was acquired from a single simulation process (re-entering mechanism was allowed).

- Small spatial clusters ($1 < n \leq 5$): The occurrence of small spatial clusters decreases monotonically as the desired velocity increases. The slope, however, appears sharp for $v_d < 2$ m/s and decreases for $v_d > 3$ m/s (approximately). The former behavior is complementary to an increment of the medium spatial clusters. Also, for $v_d > 3$ m/s the small and big spatial clusters complement each other, while no medium clusters are present. An inspection of the animations shows that the big spatial cluster always surrounds the exit where the pressure maximizes. The small spatial clusters appear at the back of the “bulk”. The

latter occur as a result of the perturbations when re-injecting pedestrians, and thus, should be considered as an artifact from the periodic boundary conditions.

- Medium spatial clusters ($5 < n < 15$): They occur at the very beginning of the *faster is slower* effect and holds for a narrow range of desired velocities (say, between $1 < v_d < 3$ (m/s)). These are responsible for the increase in the evacuation time (as already known), but even before the evacuation time arrives to a maximum, the medium size clusters vanishes.
- Big spatial clusters ($n \geq 15$): They become significant above $v_d = 2$ m/s, approximately. At this threshold, the pressure is high enough to force the pedestrians contact each other. A single big cluster would be expected to very high desired velocities.

4.4. The relation between the size of the spatial clusters and the frictional clogging delays

Recall from Section 4.2.3 that we classified the clogging delays into three categories: short ($\Delta t \leq 1$ s), intermediate ($1 \text{ s} < \Delta t \leq 3$ s) and long ($\Delta t > 3$ s). We further classified in Section 4.3.2 the size of the spatial clusters into other three categories: small ($1 < n \leq 5$), medium ($5 < n < 15$) and big ($n \geq 15$).

We now focus on the relationship between the size of the spatial clusters and the corresponding clogging delays. This relationship, however, may not be a one-to-one connection since the size of the spatial cluster can change between the beginning of a delay and the rupture of a blocking cluster (*i.e.* a subset of the spatial cluster). Thus, many spatial clusters can be reported during a *frictional clogging delay*. The number of spatial clusters (for each category) taking place between the beginning of a *frictional clogging delay* and the rupture of the corresponding blocking cluster is shown in Fig. 13.

As a first insight, it becomes clear that some kind of correlation between the size of the spatial cluster and the associated *frictional clogging delay* exists. This correlation is different for different values of the desired velocity

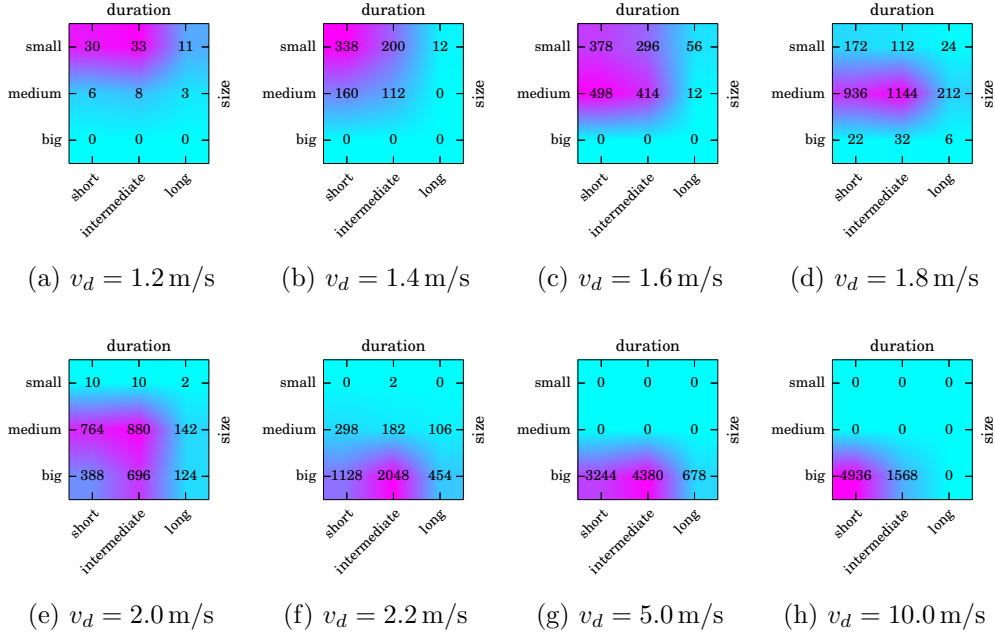


Figure 13: Tile plot between the duration of the *frictional clogging delay* and the size of the spatial cluster that produces it. In each tile the x-axis represents each of the three clogging delay categories and the y-axis represents each of the three size of the spatial cluster categories. The number inside each cell corresponds to the amount of *frictional clogging delays* that was generated by a specific spatial cluster (see text for details).

(see Fig. 13). This is in agreement with Figs. 9 and 12, since both magnitudes depend on the desired velocity. Furthermore, we can recognize two very different situations by reading the number of reported events inside each cell (see caption for details). On the upper row of Fig. 13 (plots (a) to (d)) only small and medium spatial clusters are relevant. But, on the lower row (plots (e) to (h)), the medium or big spatial clusters are the relevant ones. A closer examination, though, shows that a single size is the only relevant one in all the plots except for plots (c) and (e) ($v_d = 1.6$ and 2 m/s, respectively).

The sequence shown in Fig. 13 for increasing values of v_d may be summarized as follows:

1. The patterns (in violet) at $v_d = 1.2$ and 1.4 m/s correspond to a “two box” flat one. The same patten occurs at $v_d = 1.8$ and 2.2 to 10 m/s, but for different cluster sizes.

2. The “four box” square patterns at $v_d = 1.6$ and 2 m/s are transition patterns between two flat ones.
3. The small size category is relevant for $v_d < 1.6$ m/s. The medium size category becomes relevant for $1.6 < v_d < 2$ (m/s). The big spatial clusters are significant for $v_d > 2$ m/s.

Interestingly, Fig. 13 also shows that either the three categories of frictional clogging delays and the spatial cluster sizes are present for $v_d = 1.8$ and 2 m/s (all the cells are not empty). This means that the categories are somehow “mixed” at these desired velocities. We can find small, medium and big spatial clusters of all delays long.

Our major conclusions from this Section are as follows. First, two kinds of spatial clusters are relevant within the *faster is slower* and *faster is faster* regimes. From the point of view of the spatial clusters, small and medium spatial clusters ($n < 15$) dominate the scene for desired velocities below 3 m/s. These (almost always) match the blocking cluster definition. But, for $v_d > 3$ m/s, the giant spatial cluster ($n \geq 15$) becomes the relevant structure during the evacuation process. We may associate the overall delays (for $v_d > 3$ m/s) to the existence of this structure rather than its inner most perimeter only (say, the blocking cluster).

As a second conclusion, we noticed that (approximately) short and intermediate frictional clogging delays can be associated with small spatial clusters for low desired velocities (say, less or equal to 1.4 m/s). Besides, these clogging delays can be associated with big spatial clusters for desired velocities greater than 3 m/s. The situation in between, say $1.4 < v_d < 3$ (m/s), is somewhat mixed: two “transitions” occur at $v_d = 1.6$ and 2 m/s (approximately). The former corresponds to a small \rightarrow medium stage, while the latter corresponds to a medium \rightarrow big stage. All these regimes attain small/intermediate clogging delays.

5. Conclusions

Our research focused on the microscopic analysis of the evacuation process of self-driven particles confined in a square room with a single exit door.

We simulated 225 individuals escaping through a door with a width of two times a pedestrian width. The simulations were done in the context of the Social Force Model. We were mainly interested in properly understanding the *faster-is-slower* and *faster-is-faster* phenomena, *i.e.* the relation between the flow of pedestrians and the formation of structures (clusters) which might impede the motion of the walkers.

We have found that as the desire velocity increases, the system evolves from a condition in which the flow decreases with increasing v_d to another in which the flow increases with increasing v_d . The cause of such a change can be traced to the characteristics of the above mentioned blocking structures. We have shown that the *faster-is-slower* and the *faster-is-faster* are quite different phenomena from the standpoints of the “frictional” clogging delays and the underlying clusterization structure. The *faster-is-slower* occurs whenever the blocking clusters dominate the scene, *i.e.* there is a structure which anchors to the walls of the exit and is able to momentarily obstruct the exit, accomplishing moderate to long lasting clogging delays (say, above 1 s). However, as the v_d increases, the pressure increases as well and then, the blocking cluster becomes a giant cluster, involving (almost) all the crowd. The giant cluster is not anchored to the walls but resembles a very viscous fluid. Keep in mind that in the Social Force Model the agents are not represented by hard spheres but by soft spheres and as such the resistance opposed by the agents can be overcome by a force big enough. The harder the pedestrians push, the weaker the slowing-down, achieving the *faster-is-faster* phenomenon. This phenomenon has not been reported on other granular systems, to our knowledge.

For the set of parameters of the Social Force Model used in this work the analysis of the correlation between the clogging delays and the spatial structures showed that for $v_d > 5$ m/s, only short ($\Delta t \leq 1$ s) and intermediate ($1 \text{ s} < \Delta t \leq 3 \text{ s}$) clogging delays are produced during the giant cluster scenario. This means that the pushing efforts overcome the friction between pedestrians belonging to the “blocking” cluster, and thus, this kind of structures are not able to hold for a very long time (say, longer than 3 s). The blocking dynamic is replaced then by the collective dynamic of the giant cluster. Curiously, we noticed that short delays become increasingly relevant during the *faster-is-faster* scenario, since the burst of leaving pedestrians tends to be increasingly regular.

A by-product of our investigation is that we can distinguish between two categories of clogging delays, according to their production mechanism. The social clogging delays corresponds to those that are generated as a consequence of the social force among individuals. Instead, the frictional clogging delays are a consequence of the granular force among individual. However, social and frictional clogging delays are complementary delays whenever a blocking cluster breaks down, releasing a burst of individuals. We should call the attention on this point when analyzing the overall delay of an evacuation.

Acknowledgments

This work was supported by the National Scientific and Technical Research Council (spanish: Consejo Nacional de Investigaciones Científicas y Técnicas - CONICET, Argentina) and grant Programación Científica 2018 (UBACYT) Number 20020170100628BA. G. Frank thanks Universidad Tecnológica Nacional (UTN) for partial support through Grant PID Number SIUTNBA0006595.

Appendix A. Statistical analysis of the discharge curves

This analysis was carried out by means of the Kolmogorov-Smirnov test. This non-parametric statistical test is a goodness of fit test, which allows comparing the distribution of an empirical sample with another, or, to what is expected to be obtained theoretically (null hypothesis) [32].

The following statistic is considered

$$D_n = \max |S_n(x) - F_o(x)| \tag{A.1}$$

where $S_n(x)$ and $F_o(x)$ represent the cumulative distributions of the sampled data and the theoretical one, respectively. As can be seen, this test quantifies the maximum (absolute) difference between both distributions.

In our case, the discharge curves are compared against a uniform flow of individuals. The latter corresponds to delays of the same duration. This is useful for analyzing the relative significance of the delays during the evacuation process.

To carry out the Kolmogorov-Smirnov test, 40 discharge curves were analyzed, each of which correspond to the evacuation process of 180 individuals. The 40 selected processes were chosen separately in time, in order to be uncorrelated. The results are presented in Fig. A.14.

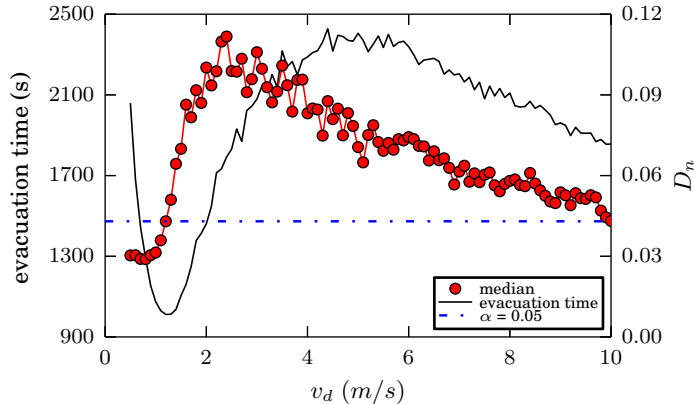


Figure A.14: The black line corresponds to the evacuation time for the first 7000 evacuees as a function of the desired velocity v_d . Red circles correspond to the Kolmogorov-Smirnov test (see text for details). The blue horizontal dashed line corresponds to a significance level of 5%. 40 discharge curves were analyzed for each desired velocity. Each discharge curve corresponds to the evacuation process of 180 individuals. These were uncorrelated sub-intervals from a single simulation process (re-entering mechanism was allowed).

As can be seen, the behavior of the median coincides qualitatively with that corresponding to the evacuation time. However, both curves are horizontally shifted from each other. The maximum of the curve corresponding to the median is approximately at $v_d = 2$ m/s, unlike what happens with the evacuation time ($v_d = 5$ m/s). It should be noted that the former occurs in the moment of the inversion of the concavity of the curve associated with the evacuation time.

We can identify two regimes from Fig. A.14, depending on the desired velocity. For $v_d < 2$ m/s, the discrepancy between the simulated and uniform flow increases as the desired velocity increases. This means that the flow becomes more irregular as the anxiety of the individuals increases. As will be seen in Section 4.3, this is due to the influence of blocking clusters during the evacuation process.

On the other hand, for $v_d > 2$ m/s, the discrepancy D_n as the desire to escape from the room increases. Thus, the flow becomes more regular. It is worth mentioning that this behavior starts during the *faster is slower* effect (and continues during the *faster is faster* effect). In addition, it is possible to notice a linear behavior of the median in this range of desired velocity.

Finally, in order to quantify the discrepancy between both distributions, a significance level of 5% is indicated in Fig. A.14 (dashed line). As can be seen, the null hypothesis is rejected for approximately the entire explored range of desired velocity. On the other hand, it should be noted that this is not possible before the minimum evacuation time (*i.e.* $v_d < 1.1$ m/s). At this interval, the individuals are actually not in contact. Therefore, the flow of evacuees occurs uninterruptedly due to the absence of blocking clusters. Thus, we can only concluded that the flow it is not uniform.

Appendix B. Blocking cluster probability

We analyze here the probability of occurrence of a blocking cluster (see Fig. B.15). That is, the percentage of time that the system is in the presence of a blocking cluster. Recall that in Fig. 6 it was observed that, for any given delay value, as the desired velocity increases, so does the probability that this delay was generated by a blocking cluster.

As can be seen, the higher the desired velocity, the greater the probability of attaining a blocking cluster. Moreover, it has an asymptotic behavior above $v_d = 5$ m/s, approximately. This means that above this desired velocity, the presence of blocking clusters is permanent over time. However, we can note that despite the still presence of a blocking cluster in front of the door, evacuation time decreases. The explanation for this phenomenon are explained in Section 4.3.

The above results are in agreement with those reported in Refs. [15, 16], in spite of the different boundary conditions, ranges of desired velocity and/or the value of the elastic constant k_n [29]. But, unlike the results reported in the literature where this behavior occurs in the presence of the *faster is slower* effect, in this case we observe that it is also satisfied during the *faster*

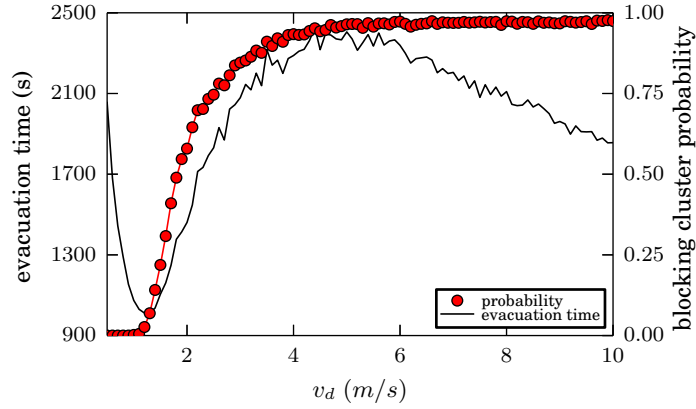


Figure B.15: The black line and red circles correspond to the evacuation time for the first 7000 evacuees and the probability of a blocking cluster as a function of the desired velocity v_d , respectively. These were computed from a single simulation process (re-entering mechanism was allowed).

is faster effect.

Besides, we were able to observe through the process animations that at the moment in which a blocking cluster is fractured, it is replaced by another immediately for $v_d > 5$ m/s (*i.e.* probability of blocking cluster equal to one). Also, the videos show that the number and composition of individuals that make up the blocking cluster changes dynamically over time. However, despite this, the presence of a blocking cluster in front of the door is permanent for $v_d > 5$ m/s.

References

References

- [1] M. Haghani, M. Sarvi, Z. Shahhoseini, When push does not come to shove: Revisiting faster is slower in collective egress of human crowds, *Transportation Research Part A: Policy and Practice* 122 (2019) 51 – 69.
- [2] W. Jianyu, M. Jian, L. Peng, C. Juan, F. Zhijian, L. Tao, M. Sarvi,

- Experimental study of architectural adjustments on pedestrian flow features at bottlenecks 2019 (8) (2019) 083402.
- [3] J. W. Adrian, M. Boltes, S. Holl, A. Sieben, A. Seyfried, Crowding and queuing in entrance scenarios: Influence of corridor width in front of bottlenecks, 2018.
 - [4] A. Garcimartín, D. R. Parisi, J. M. Pastor, C. Martín-Gómez, I. Zuriguel, Flow of pedestrians through narrow doors with different competitiveness, *Journal of Statistical Mechanics: Theory and Experiment* 2016 (4) (2016) 043402.
 - [5] W. Liao, A. Seyfried, J. Zhang, M. Boltes, X. Zheng, Y. Zhao, Experimental study on pedestrian flow through wide bottleneck, *Transportation Research Procedia* 2 (2014) 26 – 33, the Conference on Pedestrian and Evacuation Dynamics 2014 (PED 2014), 22-24 October 2014, Delft, The Netherlands.
 - [6] W. Daamen, S. Hoogendoorn, Emergency door capacity: Influence of door width, population composition and stress level, *Fire Technology* 48 (2012) 55–71.
 - [7] J. Liddle, A. Seyfried, B. Steffen, W. Klingsch, T. Rupprecht, A. Winkens, M. Boltes, Microscopic insights into pedestrian motion through a bottleneck, resolving spatial and temporal variations.
 - [8] A. Seyfried, O. Passon, B. Steffen, M. Boltes, T. Rupprecht, W. Klingsch, New insights into pedestrian flow through bottlenecks, *Transport. Sci.* 43 (2007) 395–406.
 - [9] J. Liddle, A. Seyfried, W. Klingsch, T. Rupprecht, A. Schadschneider, A. Winkens, An experimental study of pedestrian congestions: Influence of bottleneck width and length.
 - [10] A. Nicolas, S. Bouzat, M. N. Kuperman, Pedestrian flows through a narrow doorway: Effect of individual behaviours on the global flow and microscopic dynamics, *Transportation Research Part B: Methodological* 99 (2017) 30 – 43.
 - [11] N. Shiwakoti, X. Shi, Y. Zhirui, Y. Liu, J. Lin, A comparative study of pedestrian crowd flow at middle and corner exits, 2016.

- [12] J. M. Pastor, A. Garcimartín, P. A. Gago, J. P. Peralta, C. Martín-Gomez, L. M. Ferrer, D. Maza, D. R. Parisi, L. A. Pugnaloni, I. Zuriguel, Experimental proof of faster-is-slower in systems of frictional particles flowing through constrictions., *Physical review. E, Statistical, nonlinear, and soft matter physics* 92 6.
- [13] A. Garcimartn, I. Zuriguel, J. Pastor, C. Martn-Gmez, D. Parisi, Experimental evidence of the faster is slower effect, *Transportation Research Procedia* 2 (2014) 760 – 767, the Conference on Pedestrian and Evacuation Dynamics 2014 (PED 2014), 22-24 October 2014, Delft, The Netherlands.
- [14] D. Helbing, I. Farkas, T. Vicsek, Simulating dynamical features of escape panic, *Nature* 407 (2000) 487–490.
- [15] D. Parisi, C. O. Dorso, Morphological and dynamical aspects of the room evacuation process, *Physica A* 385 (2007) 343–355.
- [16] D. Parisi, C. O. Dorso, Microscopic dynamics of pedestrian evacuation, *Physica A* 354 (2005) 606–618.
- [17] I. M. Sticco, F. E. Cornes, G. A. Frank, C. O. Dorso, Beyond the faster-is-slower effect, *Phys. Rev. E* 96 (2017) 052303.
- [18] I. Sticco, G. Frank, S. Cerrotta, C. Dorso, Room evacuation through two contiguous exits, *Physica A: Statistical Mechanics and its Applications* 474 (2017) 172 – 185.
- [19] R. Hidalgo, C. Lozano, I. Zuriguel, A. Garcimartn, Force analysis of clogging arches in a silo, *Granular Matter* 15. doi:10.1007/s10035-013-0451-7.
- [20] E. T. Owens, K. E. Daniels, *Sound propagation and force chains in granular materials*, 2011.
- [21] S. Ardanza-Trevijano, I. Zuriguel, R. Arvalo, D. Maza, A topological method to characterize tapped granular media from the position of the particles.
- [22] C. Giusti, L. Papadopoulos, E. Owens, K. Daniels, D. Bassett, Topological and geometric measurements of force chain structure, *Physical Review E* 94.

- [23] L. Papadopoulos, J. G. Puckett, K. E. Daniels, D. S. Bassett, Evolution of network architecture in a granular material under compression, *Phys. Rev. E* 94 (2016) 032908.
- [24] L. Papadopoulos, M. A. Porter, K. E. Daniels, D. S. Bassett, Network analysis of particles and grains, *Journal of Complex Networks* 6 (4) (2018) 485–565.
- [25] G. Frank, C. Dorso, Room evacuation in the presence of an obstacle, *Physica A* 390 (2011) 2135–2145.
- [26] D. Helbing, P. Molnár, Social force model for pedestrian dynamics, *Phys. Rev. E* 51 (1995) 4282–4286.
- [27] A. Strachan, C. O. Dorso, Fragment recognition in molecular dynamics, *Phys. Rev. C* 56 (1997) 995–1001.
- [28] M. Mysen, S. Berntsen, P. Nafstad, P. G. Schild, Occupancy density and benefits of demand-controlled ventilation in norwegian primary schools, *Energy and Buildings* 37 (12) (2005) 1234 – 1240.
- [29] I. Sticco, G. Frank, C. Dorso, Effects of the body force on the pedestrian and the evacuation dynamics, *Safety Science* 121 (2020) 42 – 53.
- [30] F. Cornes, G. Frank, C. Dorso, High pressures in room evacuation processes and a first approach to the dynamics around unconscious pedestrians, *Physica A: Statistical Mechanics and its Applications* 484 (2017) 282 – 298.
- [31] S. Plimpton, Fast parallel algorithms for short-range molecular dynamics, *Journal of Computational Physics* 117 (1) (1995) 1 – 19.
- [32] O. S. A.G. Frodesen, H. Toefte, Probability and statistics in particle physics, Norway: Universitetsforlaget.